A Novel Monitoring Method for Belt Wear State Based on Machine Vision and Image-processing Under Varying Grinding Parameters

Nina Wang
xi'an University of Technology
guangpeng zhang (gpzhang@xaut.edu.cn)
xi'an University of Technology
Lijuan Ren
xi'an University of Technology
Wanjing Pang
xi'an University of Technology
Yongchang Li
xi'an University of Technology

Research Article

Keywords: Abrasive belt grinding, Monitoring wear condition, Image processing, Machine vision, Random forest classification

Posted Date: April 6th, 2021

DOI: https://doi.org/10.21203/rs.3.rs-377416/v1

A novel monitoring method for belt wear state based on machine vision and image-processing under varying grinding parameters

（1 School of Mechanical and Precision Instrument Engineering, Xi'an University of Technology, Xi'an 710048, China；

* Corresponding author: Guangpeng Zhang, E-mail: gpzhang@xaut.edu.cn, Tel: +08613991368732;

First author: Nina Wang, E-mail: 18792511708@163.com;

Other author: Lijuan Ren, E-mail:729770443@qq.com; Wanjing Pang, E-mail: 3050758523@qq.com;

Yongchang Li, E-mail: 1808257628@qq.com)

Abstract

The wear state of abrasive belt is one of the important factors affecting the grinding precision of belt grinding processes. Accurate monitoring of abrasive belt wear can not only provide the basis for accurate material removal model to improve grinding accuracy, but also can replace the belt to avoid surface burn in time. However, most of the existing abrasive belt wear monitoring methods are only suitable for monitoring the belt wear state under specific grinding parameters, are not universal. This paper introduces a method of belt wear state monitoring based on machine vision and image-processing. All the surface images of the belt were obtained from the new belt to the worn-out of the belt by a non-contact electron microscope. The features of abrasive belt surface images are extracted from RGB color space and wavelet texture. By analyzing the trendency of the extracted features in the whole grinding process, the wear state is divided into three categories. Three image features related to the wear state are selected: the first order distance of color component R, the entropy of horizontal subgraph, and vertical subgraph of texture feature. Based on the selected features and the random forest classification algorithm, the wear state classifier of abrasive belt is established. The performance of the classifier is verified and evaluated by using the data subset of different images. The results show that the proposed method has high recognition accuracy for the belt wear state, and the accuracy can reach 99% in the accelerated wear stage. The proposed method is suitable for the monitoring of the belt wear state by the surface images of the abrasive belt measured under different grinding parameters and different measurement parameters.

Keywords: Abrasive belt grinding · Monitoring wear condition · Image processing · Machine vision · Random forest classification

1 Introduction

As a kind of precision machining technology, belt grinding is widely used for the grinding of free-form surfaces in aerospace and naval ships area[1–3]. With the successive development of industrial field and the continuous improvement of machining precision and surface quality requirements for parts, the requirements of abrasive belt grinding accuracy are also higher and higher [4–5]. The precision of grinding process

depends on the precise material removal model which are usually affected by many factors, such as grinding parameters, workpiece parameters and abrasive belt wear status [6]. In the grinding process, grinding parameters and workpiece parameters are constant values, while the abrasive belt wear state is a dynamic amount of time variation [7]. Therefore, the accurate material removal model mainly depends on the accurate monitoring of the wear state of abrasive belt.

In order to monitor the belt wear condition of abrasive belt, it is necessary to classify the wear status. Unfortunately, as a flexible tool which consists of a large and unknown number of abrasive grains with variable and stochastic cutting geometries, the belt has no uniform wear criteria [8], unlike turning tools and milling cutters. At present, the evaluation indexes of belt wear are divided into two categories: indirect and direct evaluation [9]. The indirect evaluation is the result of the abrasive belt wear indirectly reflecting the wear state of the abrasive belt. Many scholars use indirect quantity to classify wear grades in their respective studies. HtunHtun et al. [10] and Pandiyan et al. [11] are classified into five and four wear stages according to the use time of the belt, respectively. Zhang et al. [12] and Chen et al. [13] divided the wear state of abrasive belt into initial wear stage, stable wear stage and accelerated wear stage by changing material removal rate. According to the change of grinding force in grinding process, the abrasive belt condition is divided into three stages [14]. It can be seen that there is a problem in the classification of wear grades by using the indirect evaluation. That is, the indirect classification standard is effective under the specific grinding parameters. If the grinding parameters are changed, the threshold of the partition needs to be redefined and the model needs to be re established. The method of indirect evaluation to classify the wear state of abrasive belt is not universal.

Direct evaluation, which uses inherent characteristics of abrasive belt to classify wear grade is another way to classify abrasive belt wear grad. Wang et al.[15] and Mezghani et al. [16] separately counted the average reduction height of abrasive grains on the abrasive belt and the change in the angle of the abrasive grain cutting edge to classify the abrasive belt wear. Cheng et al. [17] divides the abrasive belt wear grade into 15 levels according to the percentage of the overall quality loss of the abrasive belt. These direct evaluation for dividing abrasive belt wear grades are based on the inherent characteristics of the abrasive belt, but they are not intuitive enough. The wear area of abrasive particles on the abrasive belt directly describes the amount of abrasive belt wear, and very intuitively reflects the abrasive belt wear. However, due to the random distribution of abrasive grains and cutting edges on the abrasive belt, it is difficult to obtain the wear area on the surface of the abrasive belt. At present, the wear area of abrasive particles on the abrasive belt is measured mainly by scanning electron microscope(SEM) [18]. The major advantage of SEM is that it produces an image with excellent resolution and depth of field. SEM is one of the best methods to observe and study wear flat microstructure but it is very expensive and not practical for repeated and automated wear flat measurement because it requires the destruction of the abrasive belt in order to create a sample small

enough to fit inside the SEM chamber. So it is not usually applicable to actual engineering [19].

With the successive development of machine vision and image-processing technology, many scholars combine machine vision and image processing technology to classify and monitor wear. Arunachalam et al. [20] used a charge-coupled device (CCD) camera to acquire images of the grinding wheel at different time intervals, and used appropriate statistics and fractals to analyze the texture of the image of the grinding wheel. A method for evaluating the condition of the grinding wheel based on machine vision and the surface texture of the grinding wheel is proposed. Feng et al.[21] used industrial CCD camera to collect the grinding wheel surface image during the grinding wheel grinding process, and proposed a method of using image processing to monitor and recognize the chip loading and cutting edge wear of a grinding wheel. Stephane et al. [22] measured the surface image of the grinding wheel by CCD, and calculated the wear area of the surface of the grinding wheel using the image processing method of area growth. The calculation result is equivalent to the scanning electron microscope. It can be seen that the method of machine vision and image processing are mainly applied to the recognition the wear state of the grinding wheel, but the study of the wear of the abrasive belt using this method has not yet received attention.

After the abrasive belt wear condition is classified, it needs to be monitored. The current monitoring methods can also be divided into direct and indirect sensors monitoring [23]. In the case of the indirect sensor methods, process parameters correlated to the wear condition are monitored and then the relationship model between them is constructed to assess the wear condition. The most commonly used parameters mainly include cutting force [24], acoustic emission (AE) [25], vibration [26], current and power [27], and sound [28] etc. However, the indirect sensor monitoring is also affected by the changing of grinding parameters. The model is effective under specific model parameters, but is not universal.

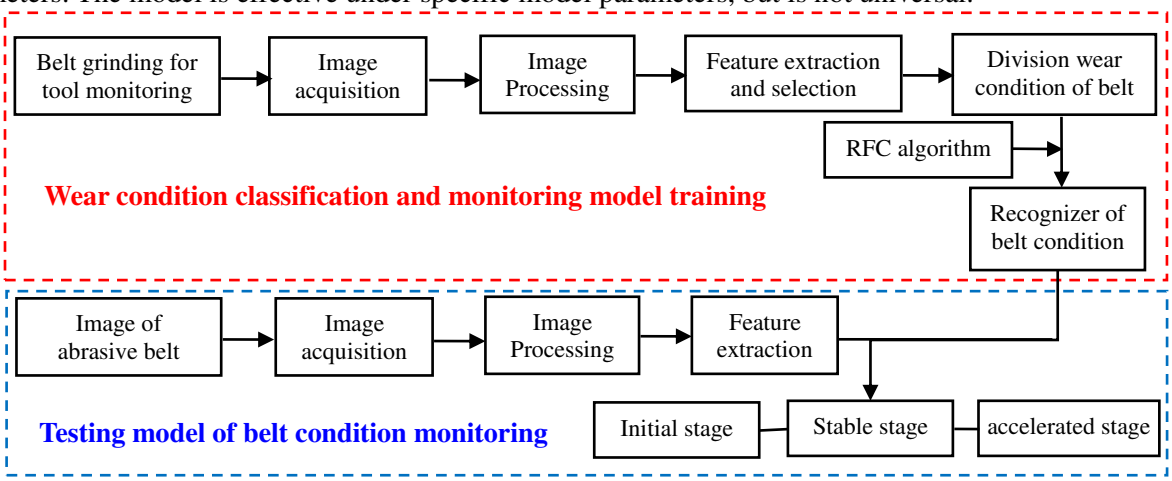

Fig. 1 The framework of belt condition monitoring

In order to solve the versatility of abrasive belt wear monitoring methods, this paper proposes a classification and monitoring method of abrasive belt wear based on machine vision and image processing. By extracting the features of contour images of the belt surface at different times, different positions and different scales in grinding process, the abrasive belt wear is divided into three stages, and a random forest

algorithm is used to establish a monitoring model of the belt wear state. The framework of belt condition monitoring based on machine vision and image-processing is shown in Fig. 1. The paper is outlined as follows: Section 1 provides an overview of the proposed abrasive grinding belt monitoring. Section 2 explains the experimental setup and method to achieve belt grain area, followed by belt surface analysis and feature extraction in Section 3. Effects of the measurement parameters on the color and texture features of the abrasive belt are analyzed in Section 4.1. And random forest classification for belt wear condition is established and recognition accuracy is analyzed in Section 4.2 and 4.3, respectively. Section 5 summarizes important conclusions of this study.

2. Experiment

2.1 Experimental setup

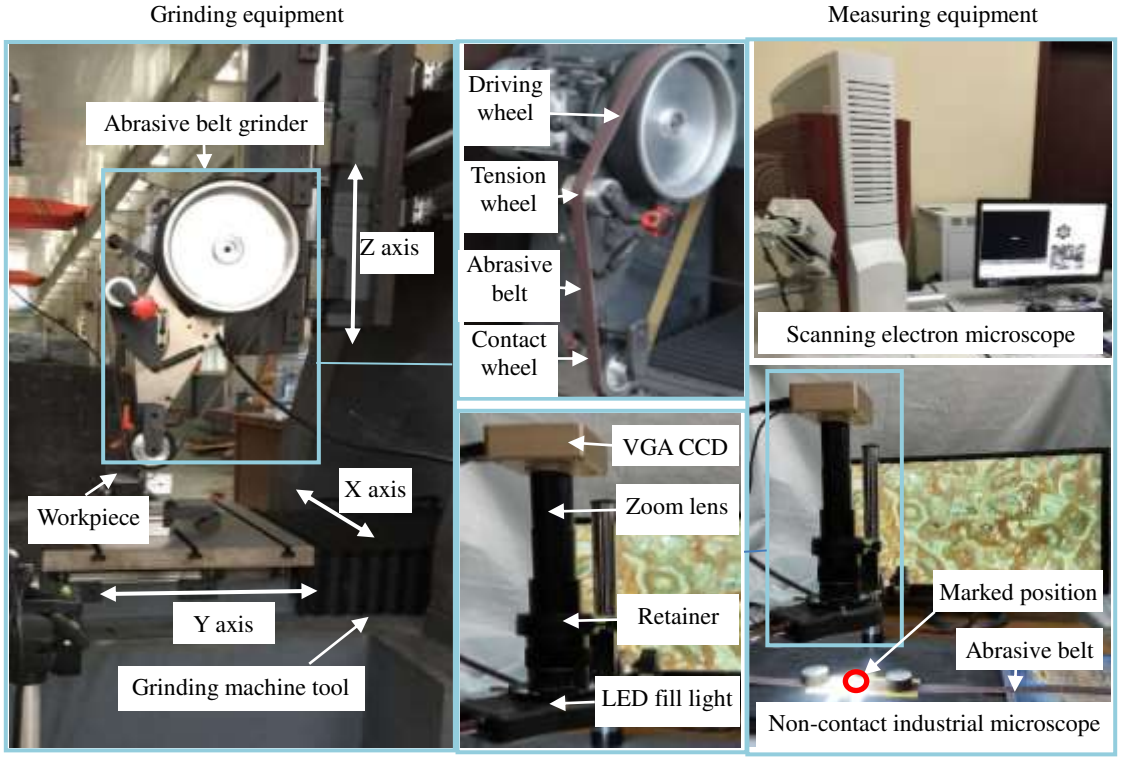

Fig. 2 Experimental setup

The experimental setup is mainly composed of grinding equipment and measuring equipment, as shown in Fig. 2. Grinding equipment includes grinding machine tool, abrasive belt grinder, and workpiece. Grinding machine tool is a three-axis (X, Y, and Z axis) grinding machine tool whose precision can reach micron level. The belt grinder is installed on the Z-axis slide of belt grinder. The abrasive belt grinder comprises a driving wheel, tension wheel, contact wheel, and abrasive belt. The driving wheel is driven with a motor having an adjustable rotational speed from 0 to 5000 rpm, and the rotational speed is converted to belt velocity from 0 to 34 m/s. The contact wheel is rubber with a Shore A hardness of 85. The width of the belt and the contact wheel is 20 mm. The belt is made using electrostatic sand-planting technology. During the experiments, each

workpiece is fixed on a worktable, and it is fed in the positive direction of the Y axis. The workpiece selects GCr15 with a hardness of HRC58. The surface of the workpiece to be machined is flat.

The measuring equipment is a non-contact industrial electron microscope(NCIEM) scanning electron microscope(EMS). NCIEM is mainly composed of HD camera, adjustable lens, led adjustable light source and display. The camera is connected to the monitor through HDMI output. And the camera adopts dual core processor, which has the characteristics of high sensitivity, low noise and smooth preview. The resolution, exposure and color of the camera can be adjusted. The lens magnification of the adjustable lens is 0.7x–4.5x, and the corresponding electronic magnification is 7x–280x. The technical parameters of the main components of the microscope are shown in Table 1.

Table 1 The main specifications of a non-contact industrial electron microscope

Index	Model	Parameters	Details
Camera	ZWSP-4800CH	High definition 48 megapixel	HDMI and sub dual output
Zoom lens	--	Eyepiece: 0.5X(Standard) Objective lense: 0.7x–4.5x	Electronic magnification 7x–280x
Lighting mode	--	LED fill light	Ring adjustable

2.2 Experiment procedure

In this experiment, two 60# brown corundum abrasive belts were used. The surface morphology images of new and worn-out belt are shown in Figs. 3 and 4. And the composition of new and worn-out abrasive belt under EDS is shown in Fig. 5. The two abrasive belts were all used for 500 cycles of grinding experiments. The parameter settings of the abrasive belt wear experiment are shown in Table 2. The grinding parameters of the first belt take grinding method 1 in Table 2, and the grinding parameters are constant. The second abrasive belt grinding parameter take grinding method 2 in Table 2, and the grinding parameter is variable. Each stroke is defined as a grinding process, starting from the contact wheel contacting the workpiece to it leaving the workpiece, and the cutting stroke is fixed at 41mm. The feed method of the grinding cycle is from the negative to the positive direction of the Y axis. The Z axis is used to ensure the theoretical grinding depth adjustment during the grinding process. Before grinding, five positions are fixed and marked on the abrasive belt, which are marked as positions No.1, 2, 3, 4, and 5, respectively. The grinding parameters are not changed in the experiment. After every 5 cycles of the belt, the different magnifications(50X, 100X, and 150X) are used to measure the surface images of the abrasive belt at previous marked position. The size of each belt image is 4608pixels*3456piexls. There are a total of 1500 abrasive belt images collected for each abrasive belt, and each picture is a sample.

We use the first one as a marking belt, which is used to classify belt wear and establish belt wear monitoring models. The second belt is used as a test belt, and the images collected by the test belt are obtained under the changed grinding parameters. The 1500 samples measured by the second belt can be divided into different feature subsets according to different measurement parameters (use time, measurement

location, and magnification). There are 15 sample sets at the same position and the same magnification, and each sample set has 100 samples. There are 5 sample sets with different magnifications at the same position, and each sample set has 300 samples. There are 3 sample sets with the same magnification in different positions, and each sample set has 500. In order to verify the feasibility of using the surface images of the abrasive belt to divide the wear state of the abrasive belt, the weight of the workpiece before and after each grinding cycle was also measured in the experiment to observe the change of the material removal rate during the entire grinding process. The measuring tool is an electronic balance with an accuracy of 0.01g.

Table 2 The parameter settings of abrasive belt wear experiment

Parameters	Values
Abrasive belt	Brown corundum-60 grit size condition: from new to worn-out
Grinding method 1	Constant grinding parameters: contact theoretical grinding depth0.3mm, belt velocity 32(m/s), and feed speed 4 (mm/s).
Grinding method 2	Variable grinding parameters: variable theoretical grinding depth0.1–0.3mm, belt velocity 14–32(m/s), and feed speed 1–8 (mm/s).
Workpiece	GCr15-170mm×41mm×50 mm-plane
Motors	The surface images of abrasive belt

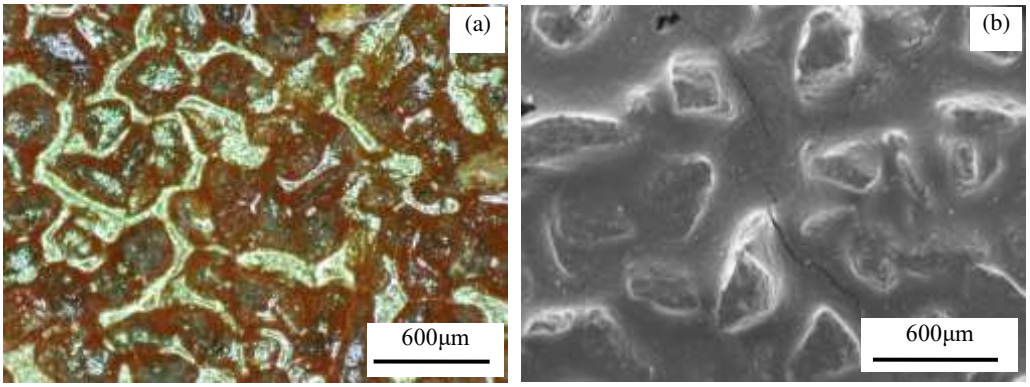

Fig. 3 The surface morphology images of 60# new abrasive belt: **a** under NCIEM, **b** under SEM

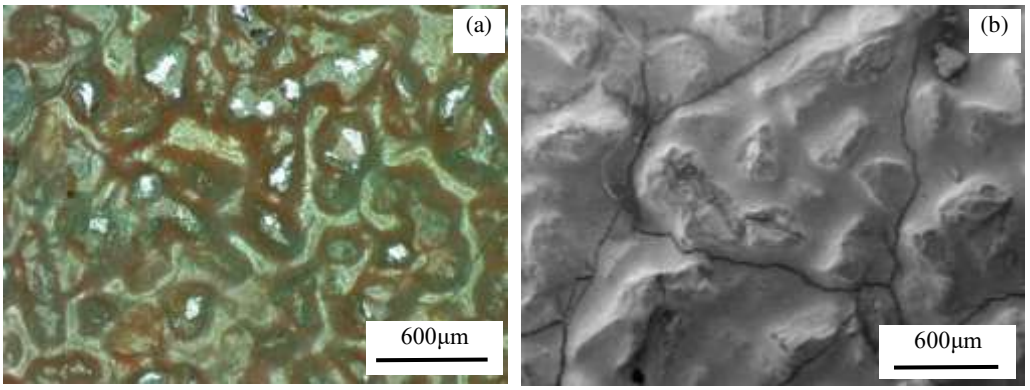

Fig. 4 The surface morphologies of 60# worn-out abrasive belt: **a** under NCIEM, **b** under SEM

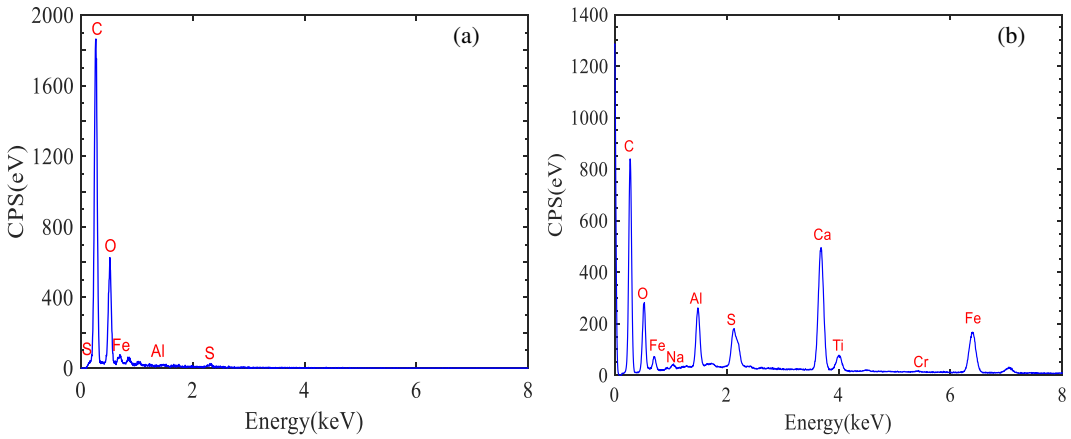

Fig. 5 EDS spectra of different wear condition: **a** new belt, **b** wear-out belt

3 Analysis and feature extraction of surface image of the abrasive belt

3.1 Analysis of the surface image of the abrasive belt

In the process of using the abrasive belt, when the abrasive grains on the abrasive belt fall off or become blunt, the abrasive belt will be invalid and need to be replaced. From the microscopic perspective of the abrasive particles on the surface of an abrasive belt, usually, there are three major types of abrasive belt grain wear: abrasive adhesion, abrasive fall-off, and blunt wear. Adhesion wear is when the chips remain on the outer surface of the abrasive grains, preventing them from continuing to cut the workpiece. Fall-off wear refers to the shedding of the abrasive particles from the binder, thereby reducing the abrasive belt grinding ability. Blunt wear indicates that there is no cutting breakage atop the abrasive grains, which reduces the material removal rate and causing burns on the surface of the workpiece.

Based on the SEM images of a 60# abrasive belt, the morphology of different types of the abrasive grains wear were observed clearly, as shown Fig. 6a. Among the three forms of blunt grinding, the two forms of sticking cover and falling off are often caused by improper selection and use of abrasive belt. Blunt wear exists in the whole wear process and is the most common form of abrasive belt wear. Fig. 6b is a surface image of the belt collected by using a NCIEM. It can be seen from the figures that the surface images of abrasive belt can clearly reflect different types of abrasive belt wear, which indicates that the abrasive belt images can effectively identify the abrasive belt wear information. The abrasive belt continues to wear during the grinding process, and the surface morphologies of the abrasive belt also changes. Fig. 7a and b show the morphologies of the abrasive belt after 220 and 425 cycles of using NCIEM. Comparing the five chosen points on the pictures, it is concluded that the wear areas of the abrasive particles increase with increase in the number of use cycles. This change can be reflected in the statistical features of the surface images of the abrasive belt. When the wear area increases, the white area of the image on the surface of the abrasive belt increases, which can be reflected by the color features and the texture features .

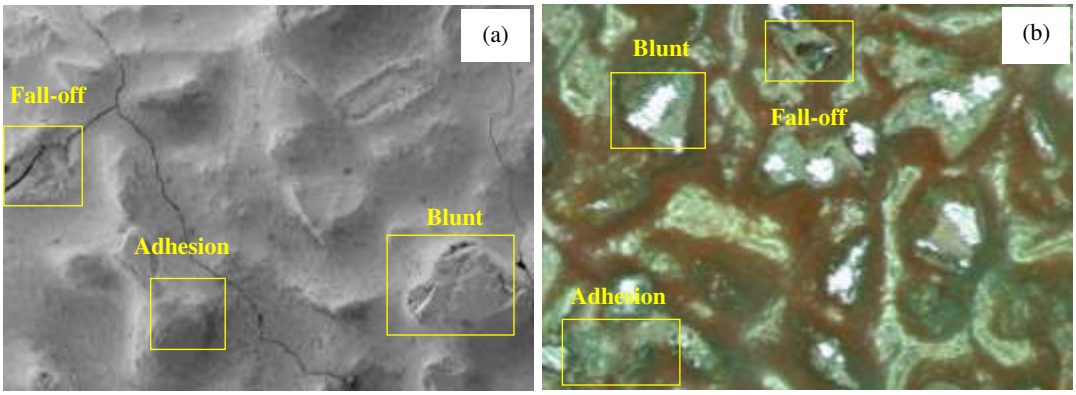

Fig. 6 Abrasive belt wear style: **a** under NCIEM, **b** under SEM

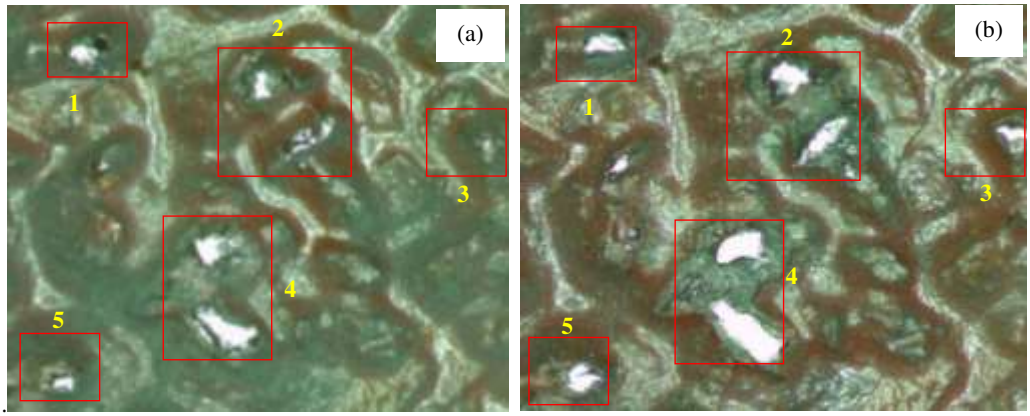

Fig. 7 The morphology of abrasive belt surface: **a** after using 220 cycles, **b** after using 425 cycles

3.2 Feature extraction of belt surface image

Analysis of Section 3.1 shows that the information related to abrasive belt wear can be reflected by the color features and texture features of the images. In order to study the laws of abrasive belt wear by the surface images of the abrasive belt, it is necessary to extract the features of the surface images of the abrasive belt. At the same time, the color features and texture features of the images are extracted to effectively describe the internal information of the images. Fig. 8 shows the RGB images of the abrasive belt surface at position No. 4 with a magnification of 50x after 405 cycles of grinding, and the corresponding color components. In order to quantify the color information of the sand belt images, the first-order distance and the second-order distance of each color component are calculated respectively, and the calculation formulas are as follows:

$$\mu_i = \frac{1}{N}\sum_{j=1}^{N} p_{i,j} \qquad (1)$$

$$\sigma_i = \left[\frac{1}{N}\sum_{j=1}^{N}(p_{i,j}-\mu_i)^2\right]^{\frac{1}{2}} \qquad (2)$$

Where $p_{i,j}$ is the i-th color component of the j-th pixel; N is the total number of image pixels. Each image sample has 6 color features.

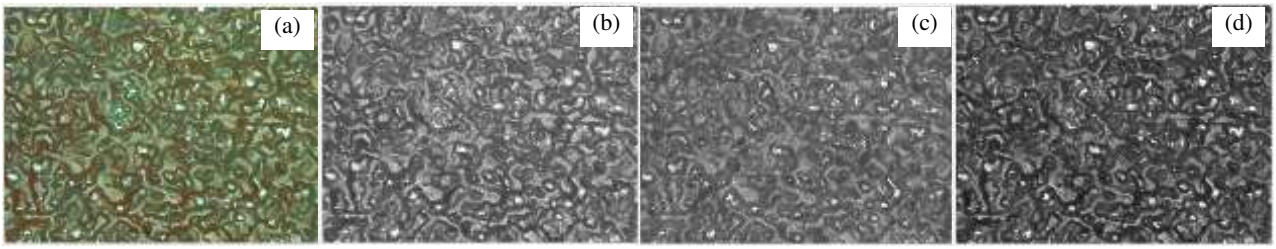

Fig. 8 The belt surface image and corresponding color components: **a** original image,**b** R color component,**c** G color component,**d** B color component

Wavelet transform can ensure that there is no information loss and redundancy in the image decomposition process, and it is widely used in image texture feature extraction [29]. This paper uses two-dimensional discrete wavelet transform to decompose the original signal into signals of different frequency bands. The decomposition process is that the original image I is filtered with low-pass L and high-pass H to form coefficient matrices I^{L} and I^{H}, and again with low-pass L and high-pass H filtering to form sub-images I^{LL}, I^{LH}, I^{HL}, and I^{HH}. Among them, I^{LL} is the original. The approximate components of the image I^{LH}, I^{HL}, and I^{HH} are the horizontal, vertical and diagonal detail components of the original image, respectively. The process of wavelet decomposition of the sand belt surface image is shown in Fig.9. The statistical features of the sub-image after the second-order decomposition are calculated as shown in Table 3. There are 6 texture features in total.

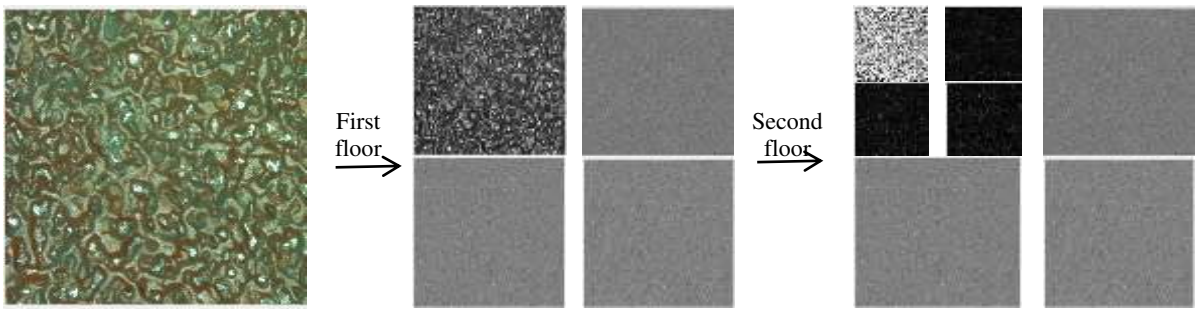

Fig. 9 Second order wavelet transform decomposition process of abrasive belt surface image

Table 3 Detail description of belt texture features

Features	Calculation formulas	Descriptions
Energy	$E=\sum_{i=1}^{M}\sum_{j=1}^{N}(p(i,j)^2)$	Reflect the uniformity of image gray distribution
Entropy	$EN=\frac{1}{M\cdot N}\sum_{i=1}^{M}\sum_{j=1}^{N}p(i,j)\log_2 p(i,j)$	Reflect the complexity of the image texture

3.3 Feature selection and wear classification

According to the sample feature extraction method in Section 3.2, we sequentially extracted 6 color features and 6 texture features of 1500 samples using MATLAB software. In order to select the features related to the abrasive belt wear conditions, we sequentially described the changes of the 12 features as the wear experiment was carried out. Fig. 10 a and b respectively show the change trend of the first-order color distance of the R component in the color feature and the entropy of the horizontal sub-image in the texture

feature. It can be seen from Fig. 10a that as the abrasive belt continues to wear, the first-order color distance of the R component increases. This is because as the blunt wear of the abrasive particles increases, the wear area of the abrasive particles continues to increase. From the perspective of image processing point, the image is getting brighter. R represents the red component in the image. The smaller the value, the lower the brightness, and the larger the value, the higher the brightness. It can be seen from Fig. 10b that as the abrasive belt continues to wear, the entropy of the horizontal subgraph decreases. This is because as the blunt wear of the abrasive grains increases, the wear area of the abrasive grains continues to increase, and the texture of the image becomes simpler and simpler.

Observing the entire threshold range of changes in color and texture characteristics, we can see that the abrasive belt wear state can be clearly divided into three stages: initial wear stage, stable wear stage and accelerated wear stage. Divided from the distribution of the number of samples, it can be seen that the boundary of the division is the 200th, near the 600th sample point. The detailed information is shown in Table 4. Fig. 11 shows the variation of the material removal rate with the grinding cycle. It can be seen that the turning points of the three wear stages are the 67th cycle and the 200th cycle respectively. Since there are three multiples for each collection, the converted sample points are divided into 66*3=198 and 200*3=600, which are basically the same as the boundary values of the sample points we divided before.

Similarly, the entropy of the vertical subgraph in the texture feature also has the same trend, and we select these three features as the feature that divides the wear state of the abrasive belt. When labeling the training data set and the test data set, two of the three features meet the division threshold of more than 2 wear levels, which will be marked as this wear level.

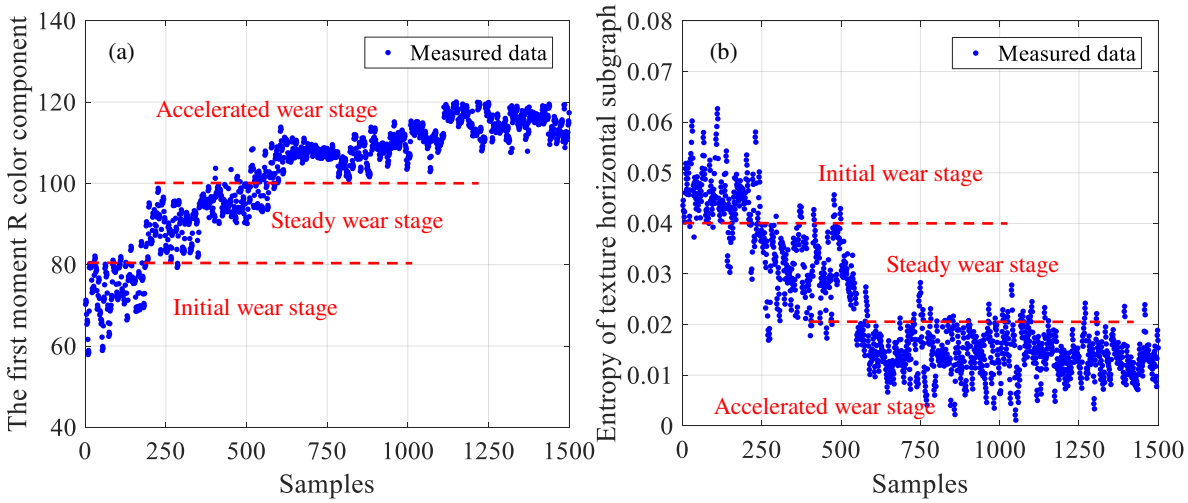

Fig. 10 The tendency of abrasive belt features: **a** color feature, **b** texture feature

Table 4 Threshold of image features on the surface of abrasive belt with different wear stages

Classification criteria	Initial wear stage	Steady wear stage	Accelerated wear stage
Samples	0–200	201–600	601–1500

The first order color distance of R component	0–80	80–100	100–
Entropy of horizontal subgraphs	0.04–	0.02–0.04	0–0.02
Entropy of vertical subgraphs	0.04–	0.02–0.04	0–0.02

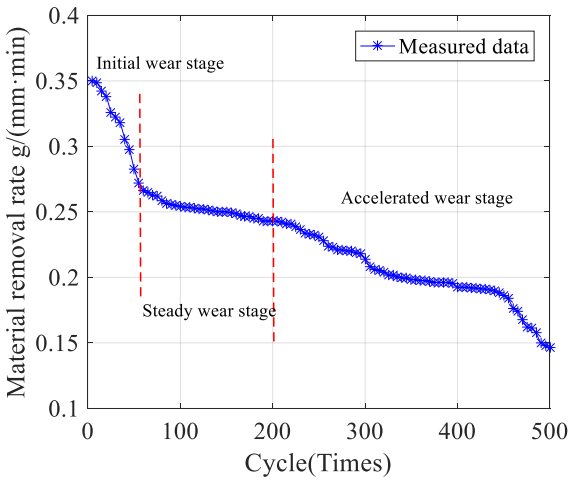

Fig. 11 The tendency of material removal rate with grinding cycles

4 The result and discussion

4.1Effects of measured parameters on belt image features

It can be seen that the wear state of the abrasive belt can be divided by color and texture features according in Fig. 11. However, the feature value of the surface images of the abrasive belt is not unique at the same time, but the value is a range of variation. This is due to the influence of different measurement time, different measurement positions, and different measurement magnifications on the image features of the abrasive belt surface during the collection process of the abrasive belt images. We denote the sand belt image features: the first-order distance of the color R component, the entropy of the horizontal sub-image, and the entropy of the vertical sub-image as features 1, 2, and 3. For different measurement parameters (use time, measurement location, and magnification), we analyze these feature values.

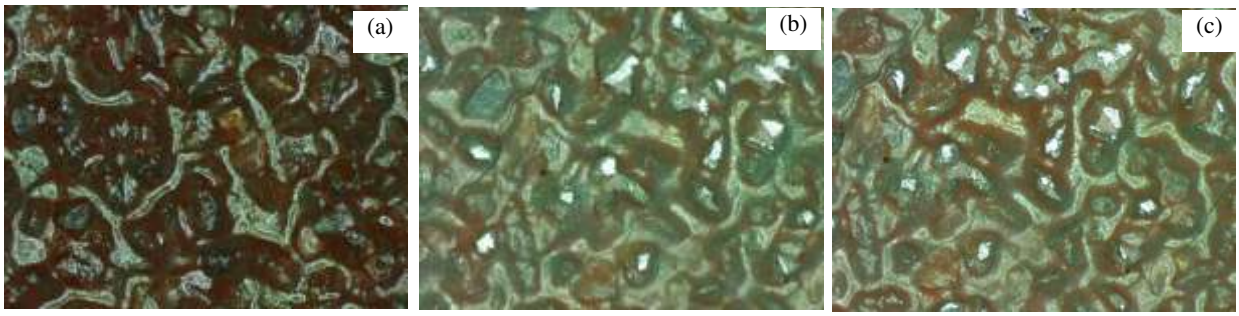

Fig. 12 The NCIEM images of abrasive belt with different using time. **a** using 60 cycle,**b** using 200 cycle,**c** using 485 cycle

Fig. 12a, b, and c are the surface images of the abrasive belt, using 150x magnification at position 1 after different using time under the NCIEM. And the corresponding image feature values are shown in Table 5. It can be seen that the values of the color features and the texture features can better distinguish the surface

images of the abrasive belt in different using time. Among the three measurement parameters, the using time is the most influential to the abrasive belt wear state, and this change can be distinguished by the surface images of the abrasive belt.

Table 5 Feature values of belt images with different using time

Features	Feature 1	Feature 2	Feature 3
Using 60 cycle	74.45	0.0474	0.0302
Using 200 cycle	107.71	0.0182	0.0230
Using 485 cycle	115.43	0.0144	0.0133

Fig. 13 shows the surface images of the abrasive belt after using 425 cycles of position 2 measured with different magnifications. The color features and texture features of the corresponding measured abrasive belt surface images are shown in Table 6. It can be seen that the color features and texture features of the surface images of the abrasive belt measured at different positions are slightly different, but the values are very close. Although the surface images of the abrasive belt measured at the same position and time under different magnifications representing the abrasive belt in the same wear state, the field of view of the measured abrasive belt is different due to the different scales. This result shows that the extracted feature values of the abrasive belt surfaces can be used for the division of the belt wear state of the abrasive belt surface images measured at different magnifications and the establishment of the recognition model.

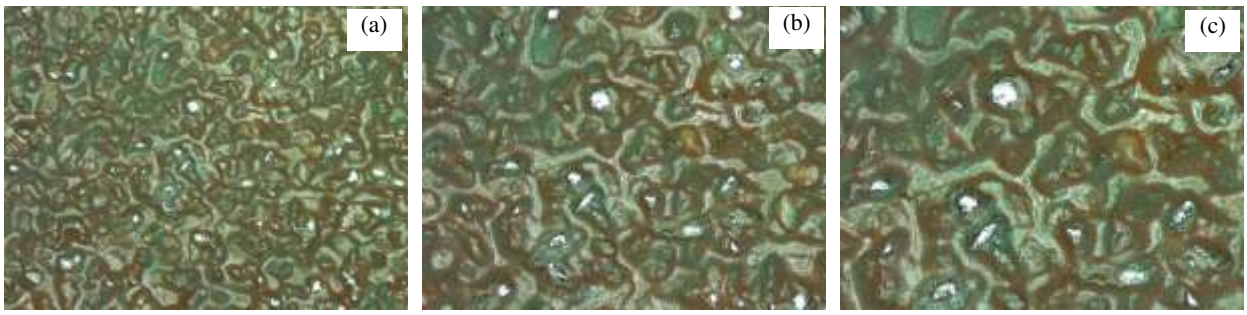

Fig. 13 The NCIEM images of abrasive belt with different magnifications: **a** 50X, **b** 100X, **c** 150X

Table 6 Feature values of belt image with different magnifications

Features	Feature 1	Feature 2	Feature 3
50x	113.32	0.0232	0.0286
100x	113.61	0.0272	0.0215
150x	112.50	0.0244	0.0243

Fig. 14 is the surface images of the abrasive belt at positions No.1, 2, and 3 measured using 150x magnification after using 465 cycles. The color features and texture features of the corresponding measured abrasive belt surface images are shown in Table 7. It can be seen that the color features and texture features of the surface images of the abrasive belt measured at different positions are slightly different, but the values are very close. This is because the surface images of the abrasive belt at the same time and the same magnification at different measurement positions represent the abrasive belt in the same wear state. It shows

that the extracted feature values of the abrasive belt surface can be used to divide the wear state of the abrasive belt surface images and to establish the recognition model for the measurement of different position measurement parameters.

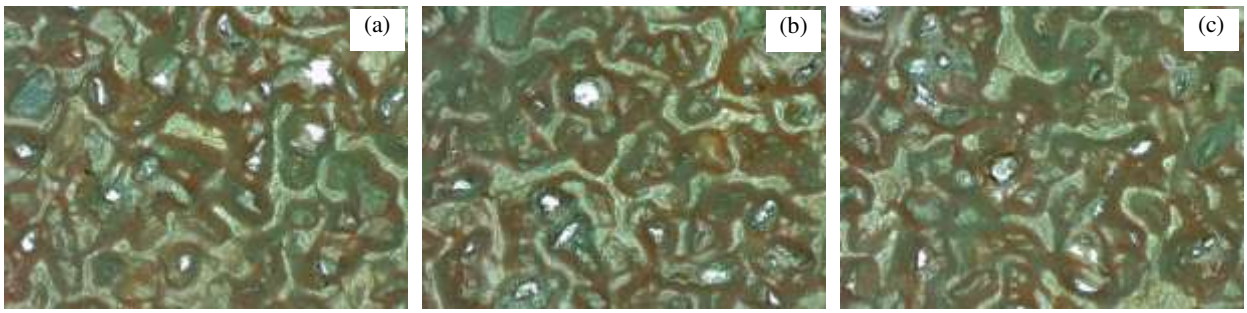

Fig. 14 The NCIEM images of abrasive belt with different marked positions. **a** position no.1,b position no.2, **c** position no.3

Table 7 Feature values of belt image with different marked positions

Features	Feature 1	Feature 2	Feature 3
Position no.1	114.06	0.0153	0.0170
Position no.2	112.50	0.0144	0.0203
Position no.3	113.86	0.0143	0.0197

Due to the experiment chose the abrasive belts using lap technology, the position of the abrasive belt joint is higher, and the wear is also more serious. Fig.15 show the surface images of the abrasive belt measured using 150x magnification after using 465 cycles at the normal measurement position 2 and the joint, respectively. The color features and texture features of the corresponding measured abrasive belt surface images are shown in Table 8. It can be seen that the lap joints position of abrasive belt are more severely worn. Compared with other positions, the color and texture features of the measured surface images of the abrasive belt are obviously different, although they represent the same wear state. Therefore, in order to ensure the accuracy and generality of the model, the overlapping position should be avoided in the process of image acquisition.

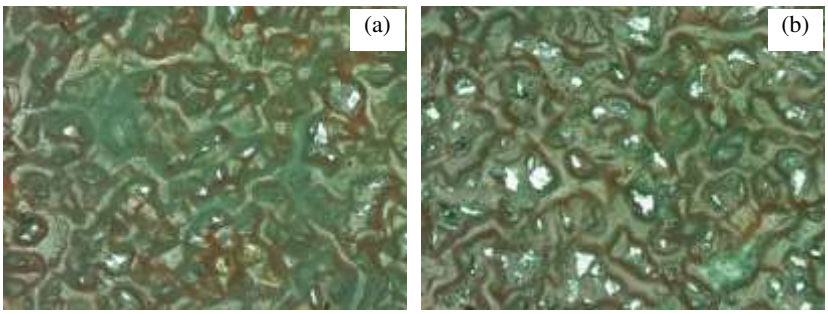

Fig. 15 The NCIEM images of abrasive belt with different positions： **a** Normal marked position, **b** joint position

Table 8 Feature values of belt images with special positions

Features	Feature 1	Feature 2	Feature 3
Normal position	105.13	0.0193	0.0187
Joint position	116.67	0.0113	0.0135

4.2 Establishment of monitoring model

4.2.1 Random Forest Classification Algorithm

Random forest is an effective ensemble learning classification algorithm. The random forest algorithm is a combination of the Bagging algorithm and the Random Subspace algorithm. The basic unit is a decision tree. The accuracy of classification is improved through the combination of multiple decision trees, and a random forest classifier is obtained. The samples of unknown categories are classified through the final voting. The schematic diagram is shown in Fig.16. In the process of establishing a random forest, there are two randomnesses. One is that the training data is randomly selected with replacement when training the decision tree。The other is that a part of the feature attributes is randomly selected during the tree splitting process, and then among them, the optimal one is selected for the split operation. Due to the introduction of these two random processes, not only the anti-noise ability of the random forest is enhanced, but also the over-fitting problem is not prone to occur.

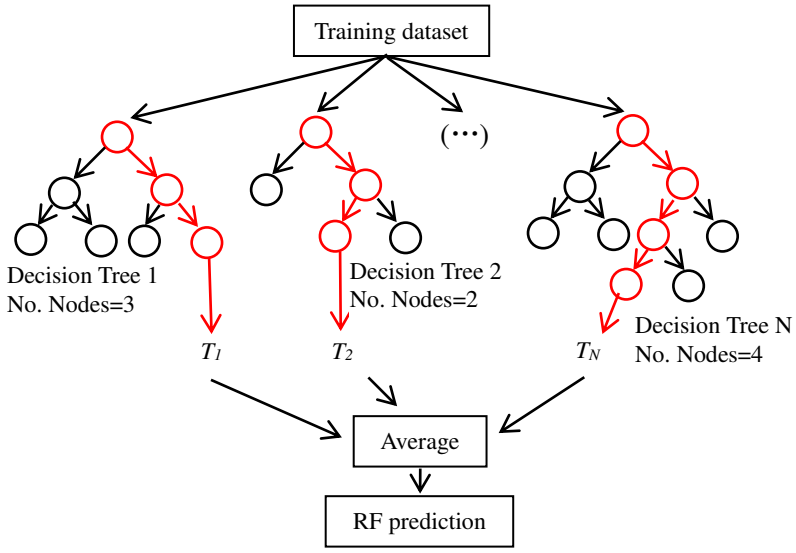

Fig. 16 Schematic diagram of random forest classification algorithm

4.2.2 Establishment of RFC-based model

Three major parameters of RFC algorithm are max-features, n-estimators, and min-sample-leaf. From the discussion in Section 3.3, the number of features is 3, and relatively small. Since every feature shows a high correlation with tool condition, all features are chosen as the inputs for every decision tree in RFC algorithm, with the maximum number of features being 3. More subtrees make the model more stable and accurate, but slow down the computation speed. Therefore, considering the performance and efficiency of the model, the n-estimator was set as 300 and the min-sample-leaf was set as 20. 1500 sets of training samples were used to train the RF model.

We used 150x magnification to collect 100 surface images of abrasive belt at different using time of position 1 as test set. In the test set, the output result is the monitoring result of abrasive belt wear state. Fig. 17a shows the test results. Fig. 17b shown a confusion matrix for abrasive belt wear status monitoring model.

The confusion matrix is used to calculate the accuracy of the abrasive belt wear status monitoring model and other evaluation indicators. 1, 2, and 3 of the abscissa and ordinate in Fig. 17 indicate the initial wear stage, the stable wear stage and the accelerated wear stage, respectively. The evaluation of the confusion matrix is shown in Table 9. It can be seen that the proposed method has a good monitoring accuracy for the abrasive belt wear state, and its accuracy can reach over 92%. In the initial wear stage and stable wear stage, the recognition accuracy is relatively low. It is because that the training data and test data in the initial wear stage and stable wear stage are less than those in the accelerated wear stage. In addition, adhesion and fall-off wear often occur in the early stage, which affects the monitoring results of belt wear in the initial wear stage.

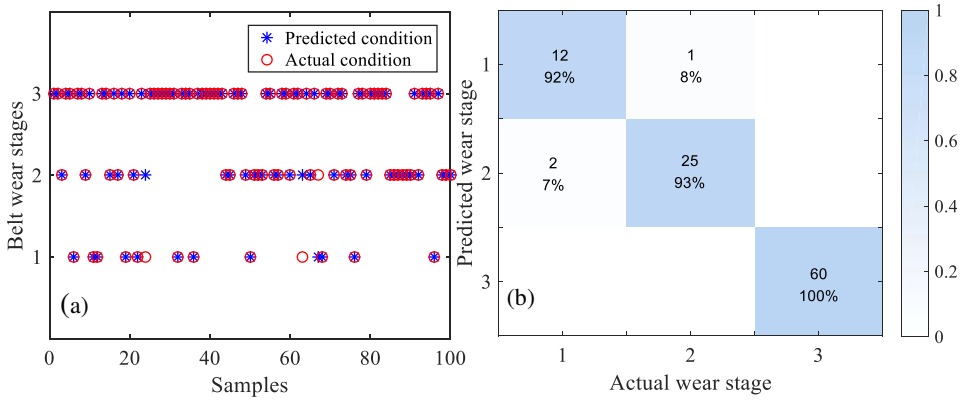

Fig. 17 Belt wear condition recognition testing result:**a** The specific values of wear stage, **b** Confusion matrix of monitoring model

Table 9 Assessment of confusion matrix

	Positive predictive value	False discover rate
Initial wear stage	92%	8%
Stable wear stage	7%	93%
Accelerated wear stage	100%	0%

4.3 Recognition accuracy of different sample sets

In order to further analyze the accuracy and universality of the recognition model for different samples, we use different test sets (300 images with different magnification at the same position and 500 images with the same magnification at different positions) to perform the model test. The prediction results and confusion matrices of images with different magnifications at the same position are shown in Fig. 18a and b, respectively. And the prediction results and confusion matrix of images with the same magnification at different positions are shown in Fig. 19a and b, respectively. The assessments of confusion matrix are shown in Table 10. The results show that the proposed method has a good accuracy for the abrasive belt surface images under different measurement parameters, and the accuracy for the test set under the same measurement parameters is the highest. When the measurement scale and measurement location are changed, the recognition accuracy decreases slightly, but the recognition accuracy in the acceleration phase exceeds 98%. In industrial applications, we usually care about the monitoring accuracy of the accelerated wear stage which usually decides whether to replace the abrasive belt.

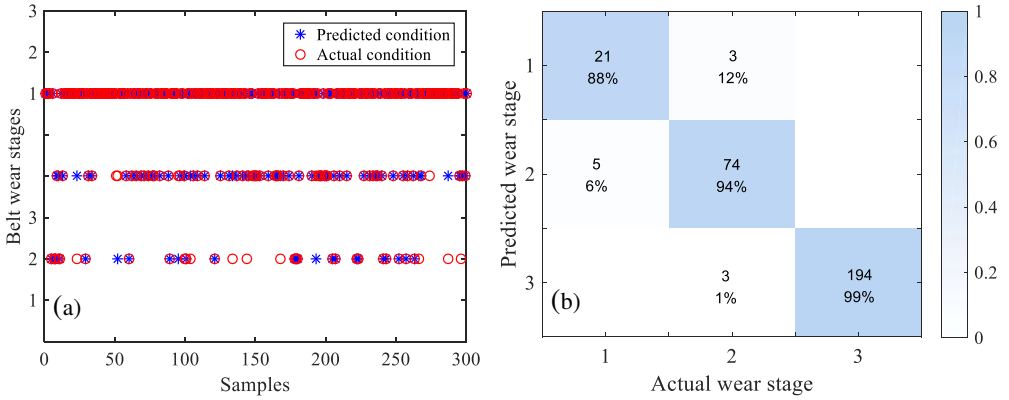

Fig. 18 Belt wear condition recognition testing result:**a** The specific values of wear stage, **b** Confusion matrix of monitoring model

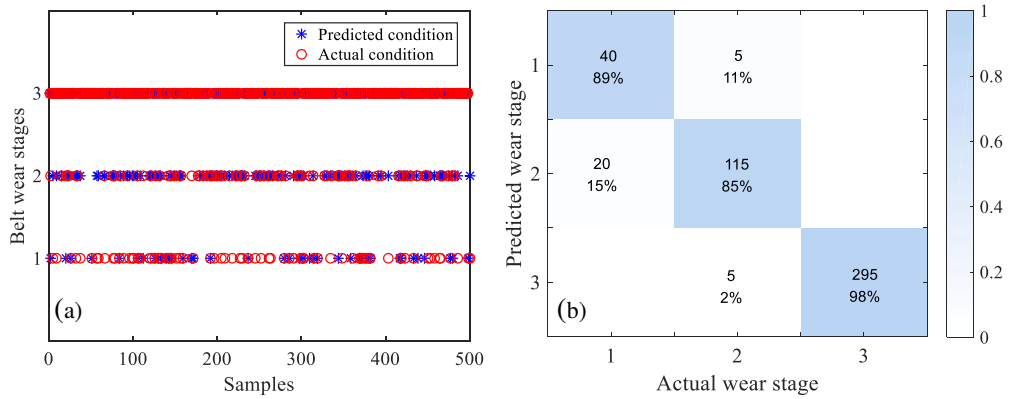

Fig. 19 Belt wear condition recognition testing result:**a** The specific values of wear stage, **b** Confusion matrix of monitoring model

Table 10 Assessment of confusion matrix

	Different magnification at the same position		Same magnification at different positions	
	Positive predictive value	False discover rate	Positive predictive value	False discover rate
Initial	88%	12%	89%	11%
Stable	6%	94%	15%	85%
Accelerated	1%	99%	2%	98%

6 Conclusions

A novel monitoring method is proposed based on machine vision and image processing for abrasive belt wear condition. This method uses the transformation range of the image features of the abrasive belt during the entire service life of the abrasive belt, and classifies the abrasive belt wear condition into three stages. Combining the surface image features of the abrasive belt and the random forest classification algorithm, a monitoring model of the abrasive belt wear state is established. The results are summarized as follows:

(1) According to the color and texture features in the abrasive belt images, the correlation between the abrasive belt wear and the image features is established, and the abrasive belt wear condition is classified.

(2) By analyzing the influence of different measurement parameters on the features of the abrasive belt surface image, it is concluded that the proposed method in this paper can be applied to the monitoring of

abrasive belt wear on the abrasive belt surface image collected by different measurement parameters.

(3) Based on the selected image features and integrated RFC algorithm, a monitoring model for abrasive belt wear is established. Using different test samples, it is concluded that the proposed method has a monitoring accuracy of over 88% of the abrasive belt wear stages, and the prediction of accelerated wear can reach 99%.

(4) The method proposed in this paper is used to monitor the abrasive belt wear condition under different grinding parameters and different measurement parameters. The combination of visual sensor technology, machine learning algorithm and image processing method improves the accuracy of the life prediction of the abrasive belt.

Declaration:

-Ethical Approval: All data in this paper comes from machining grinding experiments,and does not involve ethical issues.

-Consent to Participate: Not applicable.

-Consent to Publish: Not applicable.

-Authors Contributions: Nina Wang performed the analysis and summary of the experimental data, and was a major contributor in writing the manuscript. Lijuan Ren, Nina Wang and Wanjing Pang participate in carrying out grinding experiments. All authors read and approved the final manuscript.

-Funding:This work was supported by the Shaanxi Province key projects (grant number 2017ZDXM-GY-133).

-Competing Interests:The authors declare that they have no competing interests

-Availability of data and materials:The datasets used or analysed during the current study are available from the corresponding author on reasonable request.

References

[1] Jourani A., Dursapt M., Hamdi H., Rech J., Zahouani H. (2005) Effect of the belt grinding on the surface texture: Modeling of the contact and abrasive wear. WEAR 259(7–12):1137–1143.

[2] Recha J., Kermouchea G., Grzesikb W., Garcıa-Rosales C., Khellouki A., Garcıa-Navas V. (2008) Characterization and modelling of the residual stresses induced by belt finishing on a AISI52100 hardened steel. J Mater Process Tech 208:187–95.

[3] Fan W.G., Wang W.X., Wang J.D., Zhang X.L., Qian C., Ma T.F. (2021) Microscopic contact pressure and material removal modeling in rail grinding using abrasive belt. P I Mech Eng B-J Eng 235(1–2):3–12.

[4] Huang Y., He S., Xiao G.J., Li W., Jiahua S.L.,Wang W.X. (2020) Effects research on theoretical-modelling based suppression of the contact flutter in blisk belt grinding. J Manuf Process 54:309–317.

[5] Lv Y.J., Peng Z., Qu C., Zhu D.H. (2020) An adaptive trajectory planning algorithm for robotic belt grinding of bladeleading and trailing edges based on material removal profile model. ROBOT CIM-INT MANUF 6:101978.

[6] Vigneashwara P., Tegoeh T. (2019) Use of acoustic emissions to detect change in contact mechanisms caused by tool wear in abrasive belt grinding process. Wear 436–437:203047.

[7] Pandiyan V., Shevchik S., Wasmer K., Castagnec s., Tjahjowidodod T. (2020) Modelling and monitoring of abrasive finishing processes using artificial intelligence techniques: A review. J Manuf Process 57:114–135.

[8] Feng J., Kim B.S., Shih A., Ni J. (2009) Tool wear monitoring for micro-end grinding of ceramic materials. J Mater Process Tech 209(11):5110–6.

[9] Yang Z., Yu Z. (2013) Experimental study of burn classification and prediction using indirect method in surface grinding of AISI 1045 steel. Int J Adv Manuf Technol 68(9):2439–49.

[10] Oo H., Wang W., Liu Z.H. (2020) Tool wear monitoring system in belt grinding based on image-processing techniques. Int J Adv Manuf Technol 170(2):6254.

[11] Pandiyan V., Caesarendra W., Tjahjowidodo T., Tan H.H. (2018) In-process tool condition monitoring in compliant abrasive belt grinding process using support vector machine and genetic algorithm. J Manuf Process 31:199–213.

[12] Zhang X.Q., Chen H.B., Xu J.J., Song X.F., Wang J.W., Chen X.Q. (2018) A novel sound-based belt condition monitoring method for robotic grinding using optimally pruned extreme learning machine. J Mater Process Tech 260:9–19.

[13] Chen J.Q. , Chen H.B. , Xu J.J. , Wang J.W., Zhang X.Q., Chen X.Q. (2018) Acoustic signal-based tool condition monitoring in belt grinding of nickel-based superalloys using RF classifier and MLR algorithm. Int J Adv Manuf Technol 98:859–872.

[14] Kwak J.S., Ha M.K. (2004) Detection of dressing time using the grinding force signal based on the discrete wavelet decomposition. Int J Adv Manuf Technol 23(1–2):87–92.

[15] Salgado D.R., Alonso F.J. (2007) An approach based on current and sound signals for in-process tool wear monitoring. Int J Mach Tools Manuf 47:2140–2152.

[16] Khellouki A., Rech J., Zahouani H. (2007) The effect of abrasive grain's wear and contact conditions on surface texture in belt finishing.Wear 263(1):81–87.

[17] Cheng C., Li J.Y., Liu Y.M., Nie M., Wang W.X. (2019) Deep convolutional neural network-based in-process tool condition monitoring in abrasive belt grinding. Comput Ind 106:1–13.

[18] Fan K.C., Lee M.Z., Mou J.I. (2002) On-line non-contact system for grinding wheelwear measurement. Int J AdvManuf Technol 19(1): 14–22.

[19] Amir M.T., Zhao H.L., Henri C., Bruce H., Marin L. (2015) Characterization of grinding wheel grain

topography under different robotic grinding conditions using confocal microscope. Int J Adv Manuf Technol 80(5–8):1159–1171.

[20] Feng Z., Chen X. (2007) Image processing of grinding wheel surface. Int J Adv Manuf Technol 32:27–33.

[21] Arunachalam N. , Ramamoorthy B. (2007) Texture analysis for grinding wheel wear assessment using machine vision. P I Mech Eng B-J Eng 221(3):419-430.

[22] Stéphane L., Bauer R., Warkentin A. (2004) Application of region growing method to evaluate the surface condition of grinding wheels. Int J Mach Tools Manuf 44(7–8):823–829.

[23] Jourani A., Hagege B., Bouvier S., Bigerelle M., Zahouani H. (2013) Influence of abrasive grain geometry on friction coefficient and wear rate in belt finishing. Tribol Int 59:30–7.

[24] Feng J., Kim B.S., Shih A., Ni J. (2009) Tool wear monitoring for micro-end grinding of ceramic materials. J Mater Process Tech 209(11):5110–6.

[25] Han X.S.,Wu T.Y. (2013) Analysis of acoustic emission in precision and high-efficiency grinding technology. Int J Adv Manuf Technol 67(9):1997–2006.

[26] Wu D., Jennings C., Terpenny J., Gao R.X., Kumara S. (2017) A comparative study on machine learning algorithms for smart manufacturing: tool wear prediction using random forests. J Manuf Sci Eng 139(7):071018.

[27] Tian Y., Liu F., Wang Y., Wu H. (2017) Development of portable power monitoring system and grinding analytical tool. J Manuf Process 27:188–97.

[28] Ghosh N., Ravi Y., Patra A., Mukhopadhyayc S., Pauld S., Mohantyd A.R., Chattopadhyayd A.B. (2007) Estimation of tool wear during CNC milling using neural network-based sensor fusion. Mech Syst Signal Pr 21(1):466–79.

[29] Breiman L (2001) Random forests. Machine Learning Journal 45(1):5–32.

[30] Han XS,Wu TY (2013) Analysis of acoustic emission in precision and high-efficiency grinding technology. Int J Adv Manuf Technol 67(9):1997–2006.

Figures

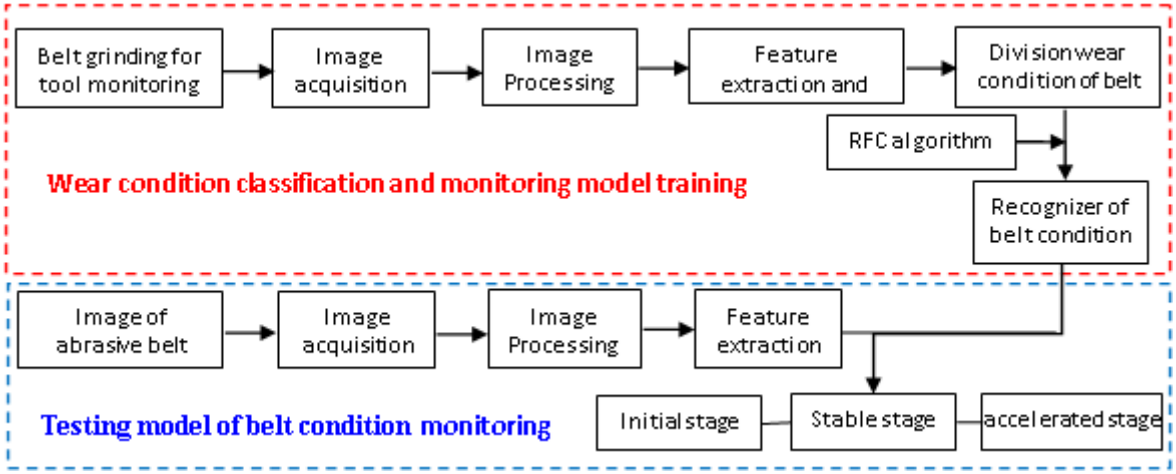

Figure 1

The framework of belt condition monitoring

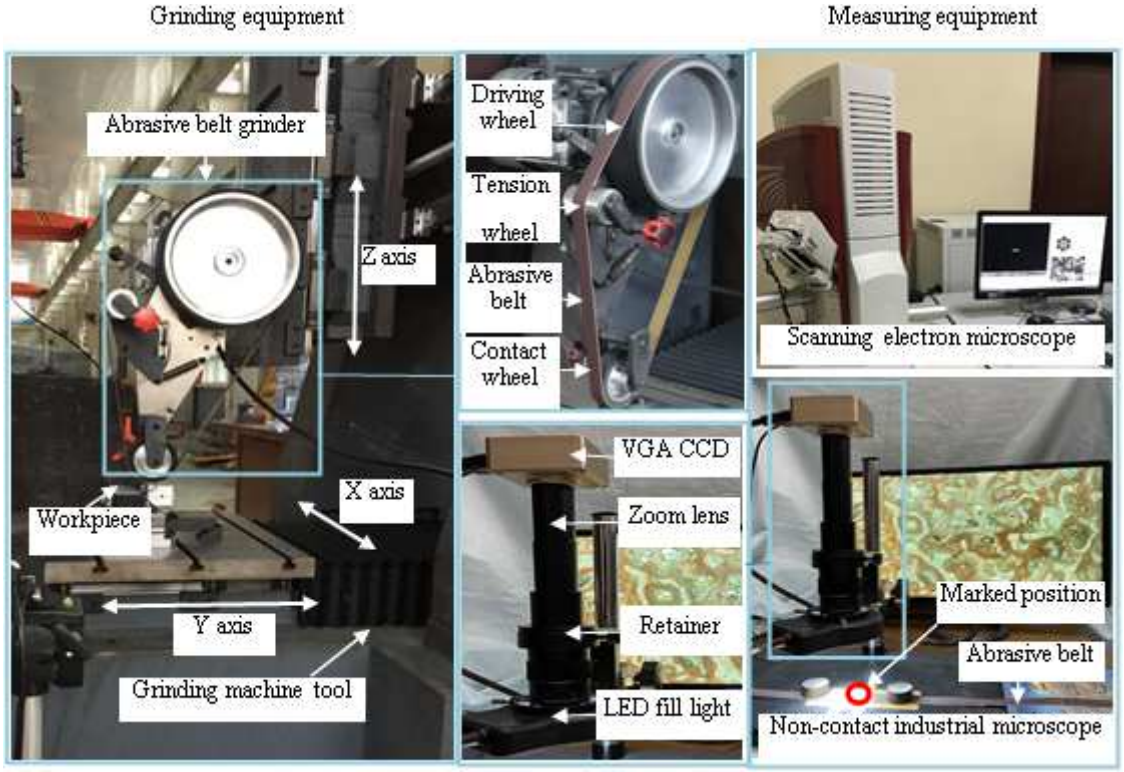

Figure 2

Experimental setup

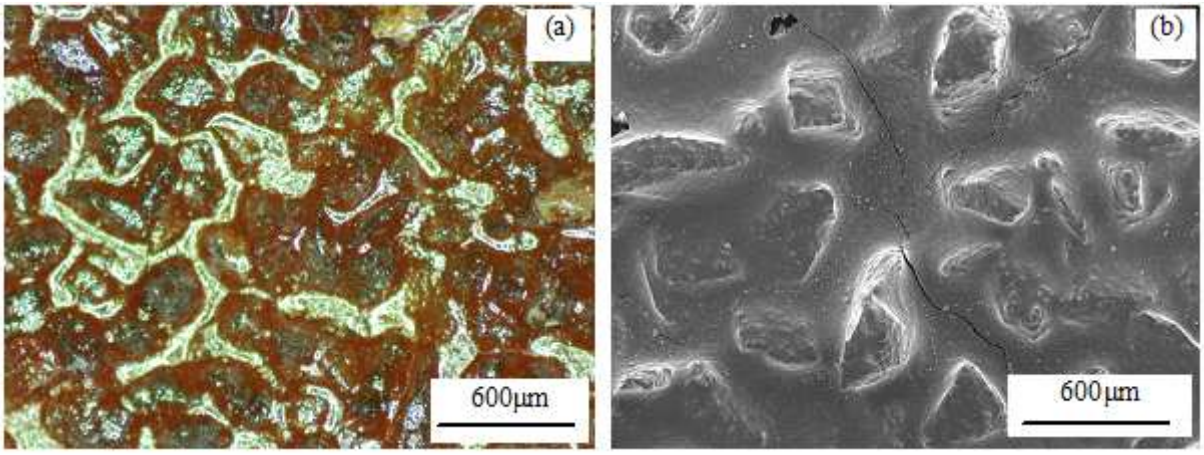

Figure 3

The surface morphology images of 60# new abrasive belt: a under NCIEM, b under SEM

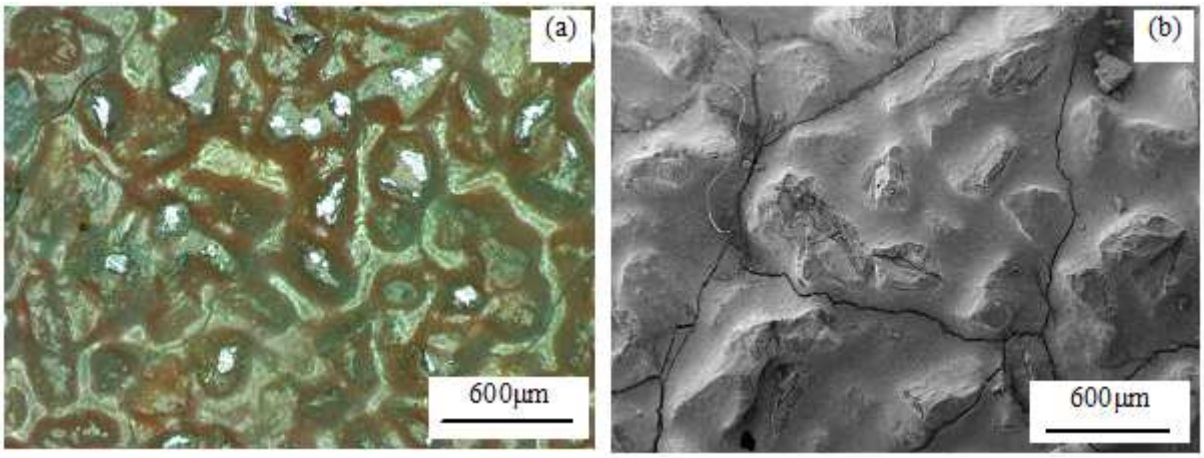

Figure 4

The surface morphologies of 60# worn-out abrasive belt: a under NCIEM, b under SEM

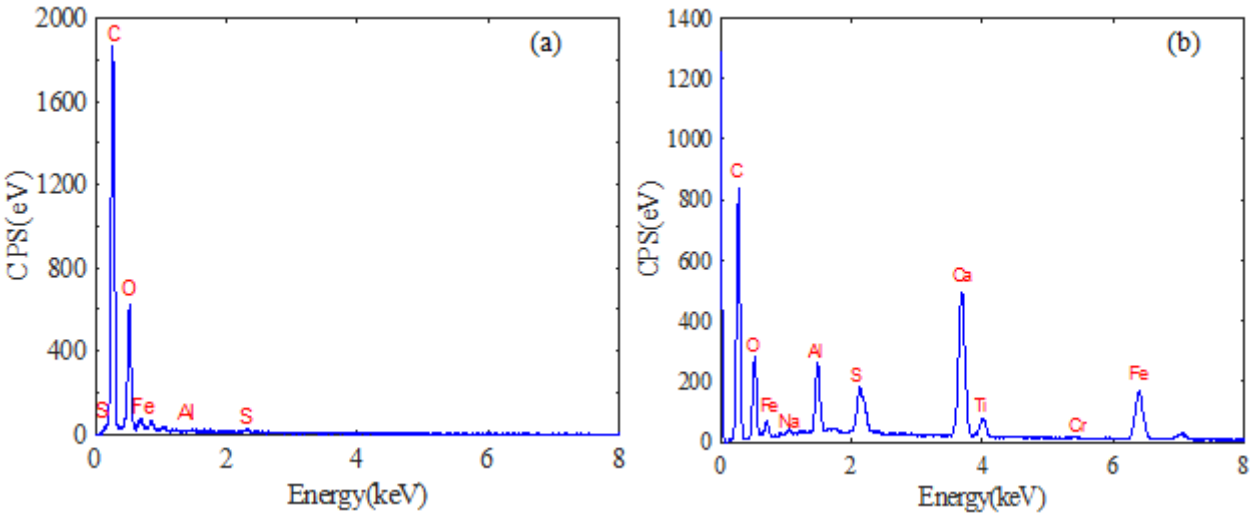

Figure 5

EDS spectra of different wear condition: a new belt, b wear-out belt

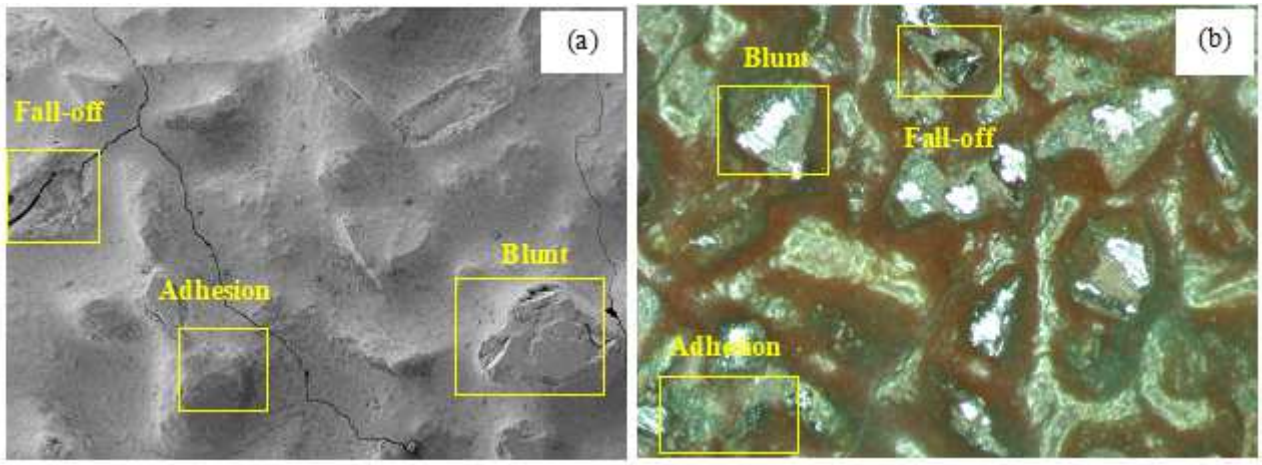

Figure 6

Abrasive belt wear style: a under NCIEM, b under SEM

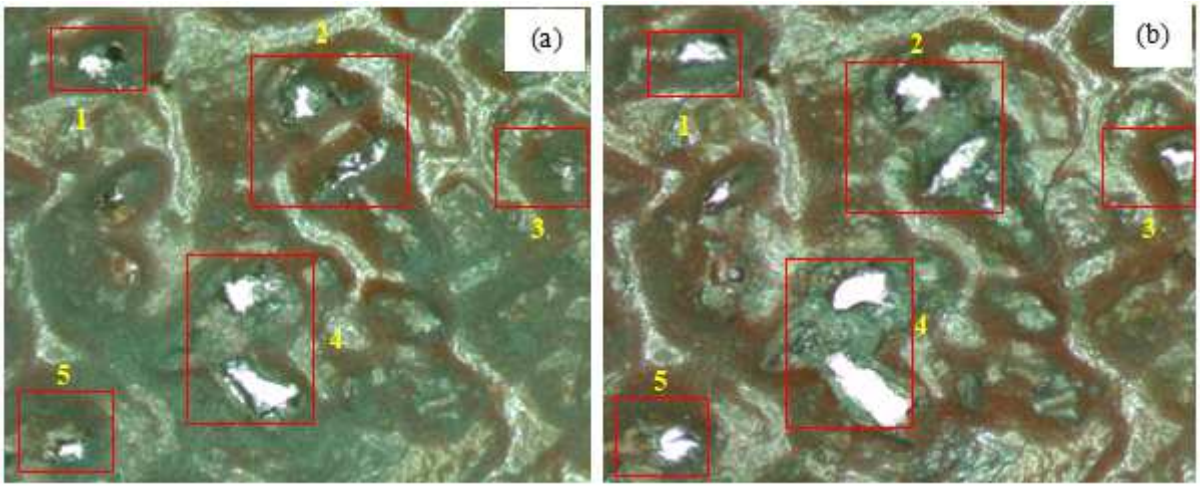

Figure 7

The morphology of abrasive belt surface: a after using 220 cycles, b after using 425 cycles

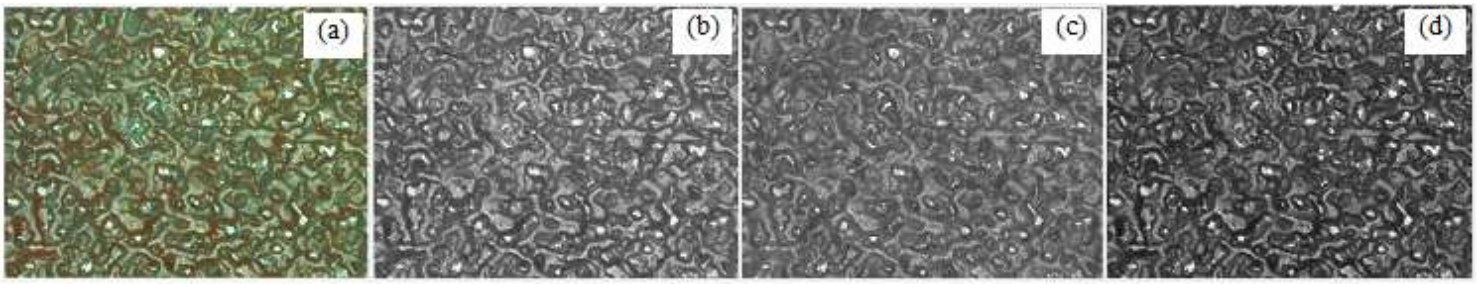

Figure 8

The belt surface image and corresponding color components: a original image,b R color component,c G color component,d B color component

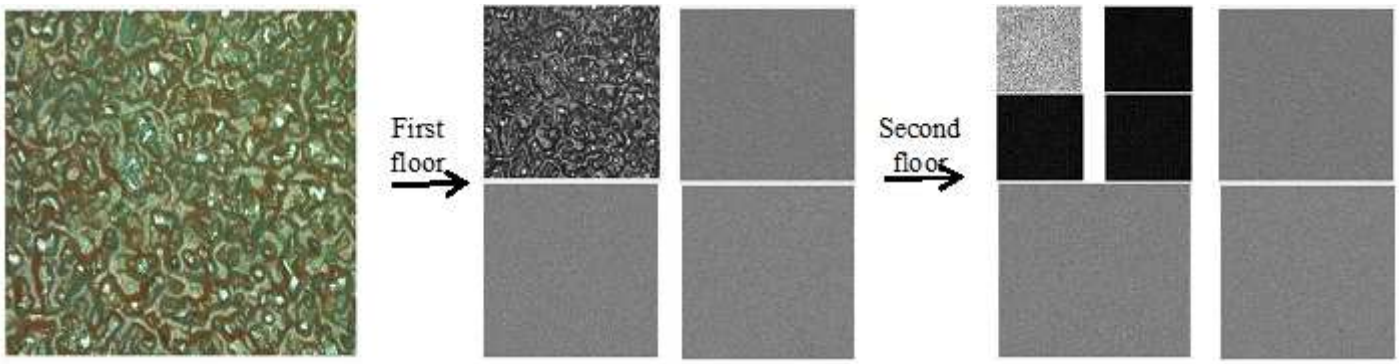

Figure 9

Second order wavelet transform decomposition process of abrasive belt surface image

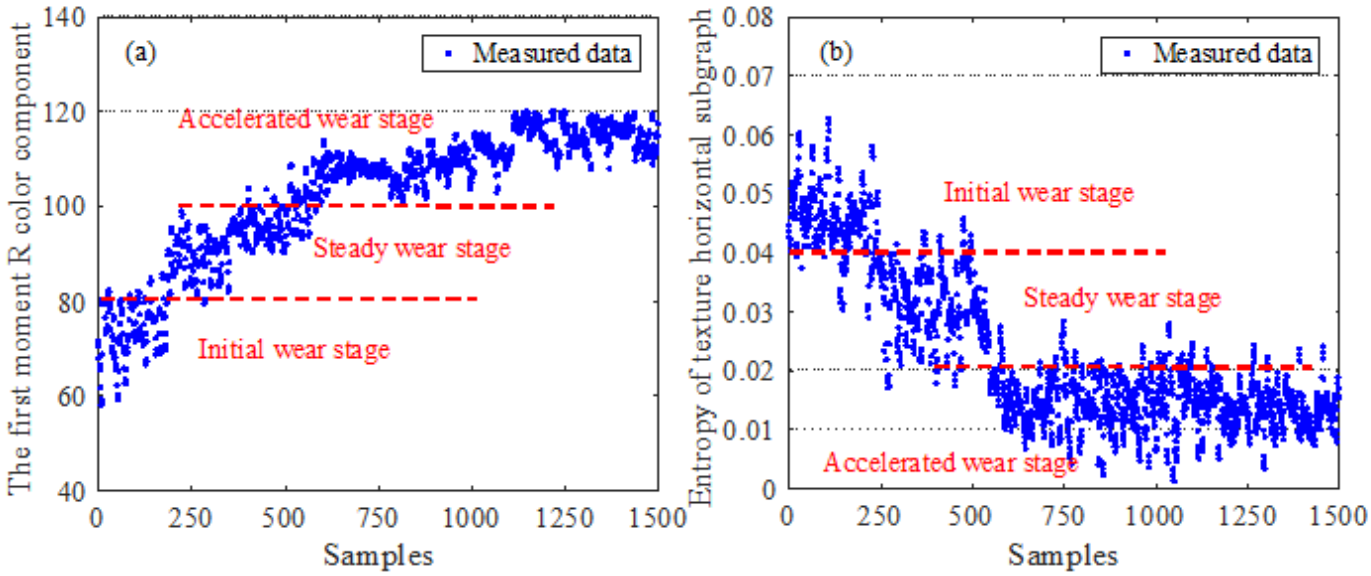

Figure 10

The tendency of abrasive belt features: a color feature, b texture feature

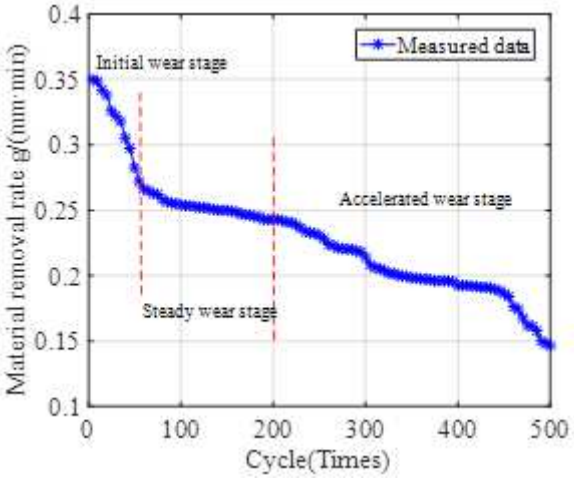

Figure 11

The tendency of material removal rate with grinding cycles

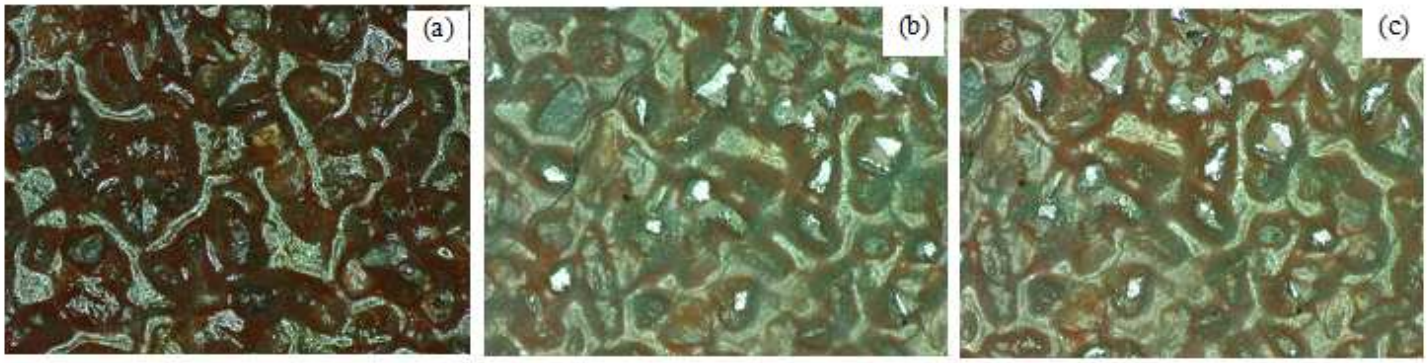

Figure 12

The NCIEM images of abrasive belt with different using time. a using 60 cycle,b using 200 cycle,c using 485 cycle

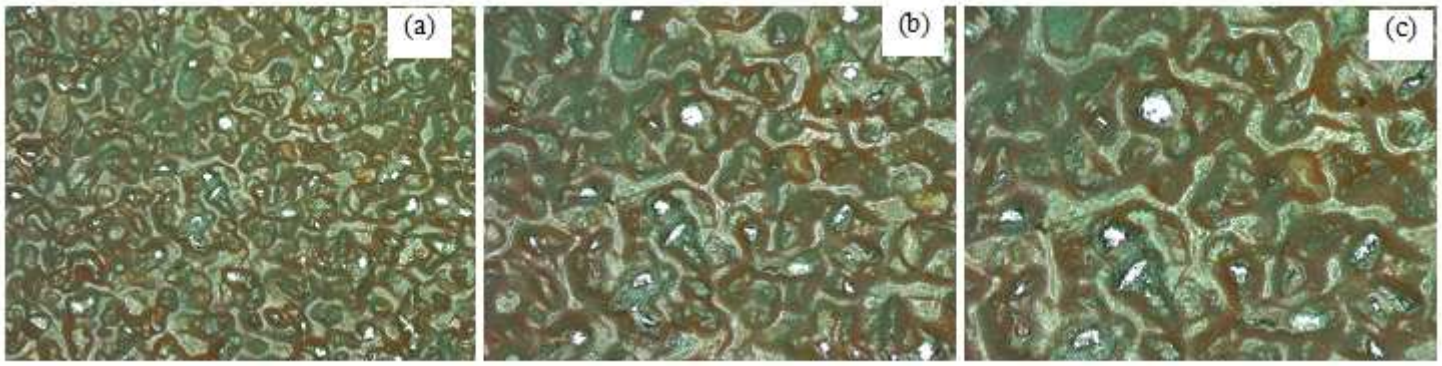

Figure 13

The NCIEM images of abrasive belt with different magnifications: a 50x, b 100x, c 150x

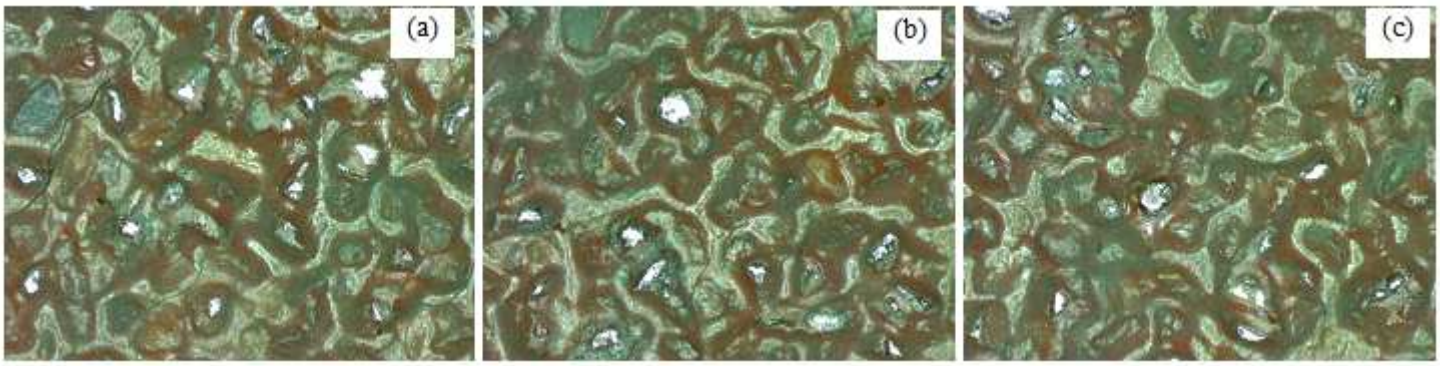

Figure 14

The NCIEM images of abrasive belt with different marked positions. a position no.1,b position no.2, c position no.3

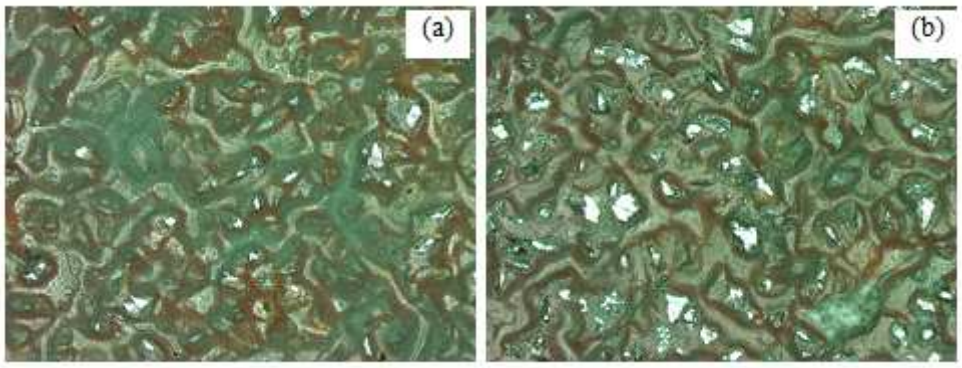

Figure 15

The NCIEM images of abrasive belt with different positions a Normal marked position, b joint position

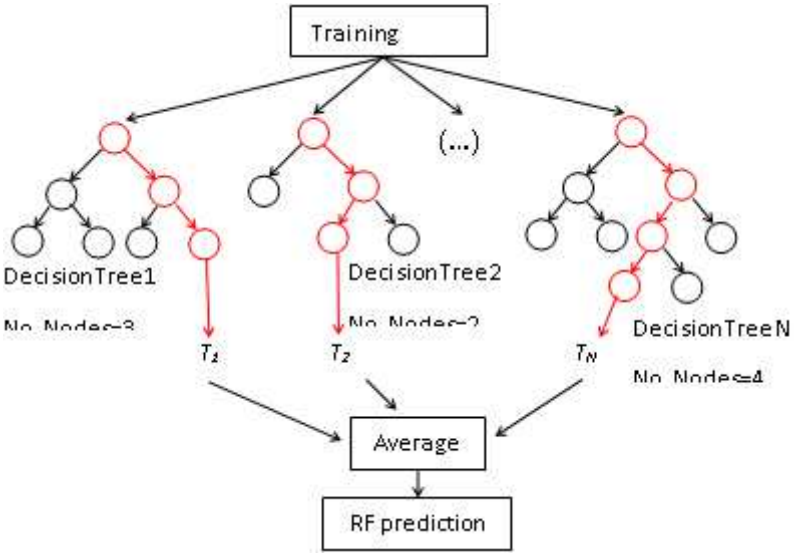

Figure 16

Schematic diagram of random forest classification algorithm

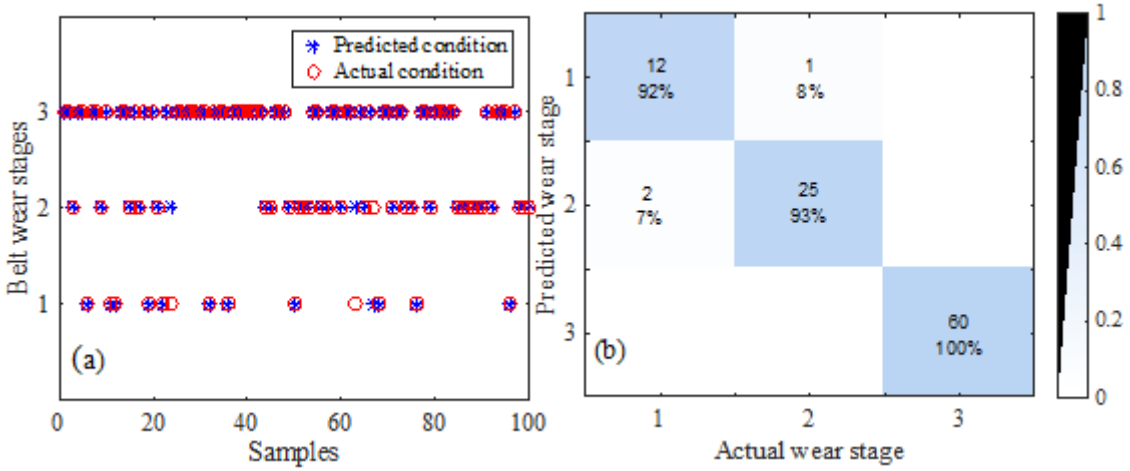

Figure 17

Belt wear condition recognition testing result:a The specific values of wear stage, b Confusion matrix of monitoring model

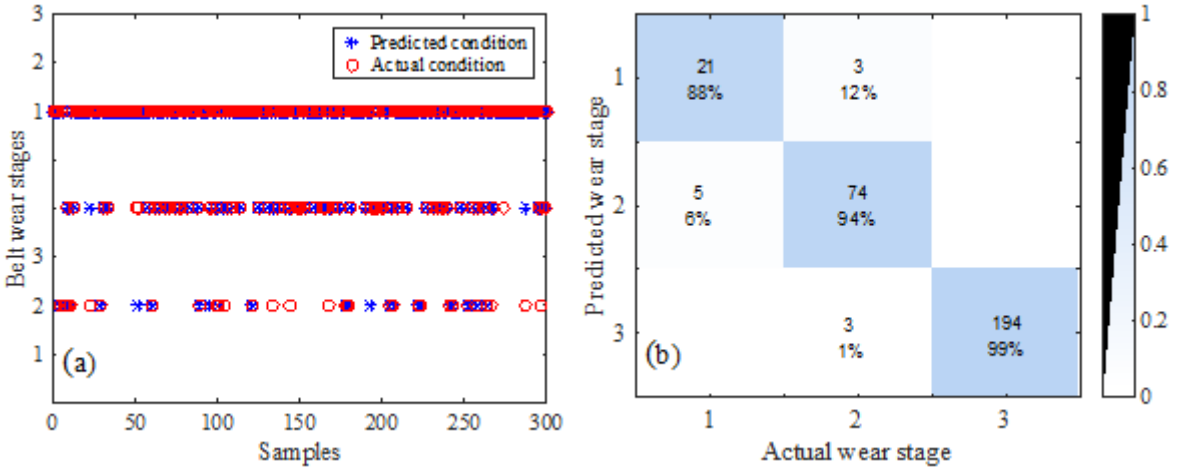

Figure 18

Belt wear condition recognition testing result:a The specific values of wear stage, b Confusion matrix of monitoring model

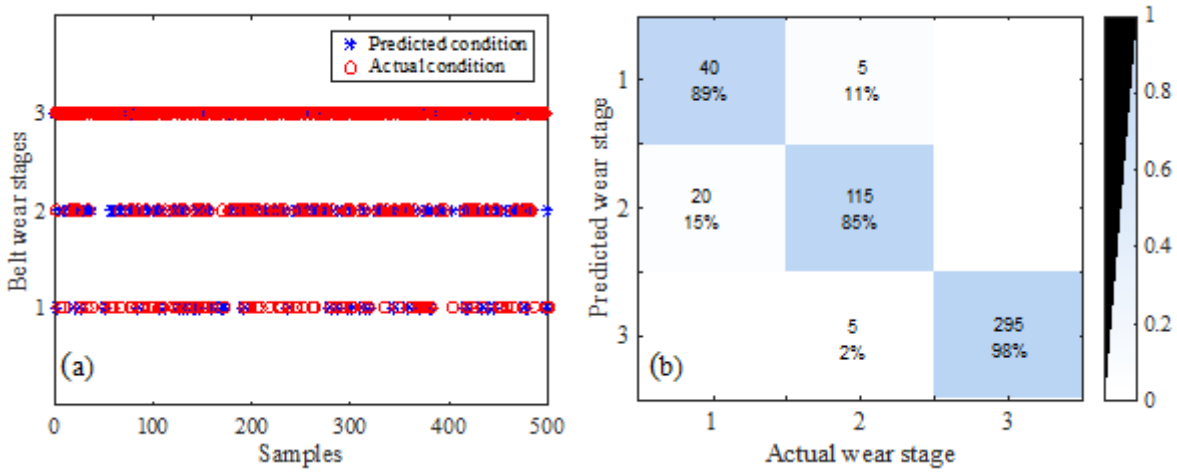

Figure 19

Belt wear condition recognition testing result:a The specific values of wear stage, b Confusion matrix of monitoring model